Effect of doping concentration on the performance of 2.8 μm Er:CaF 2 lasers

Venkatesan Jambunathan, Simone Normani, Pavel Loiko, Karel Veselský, Liza Basyrova, Abdelmjid Benayad, Patrice Camy, Ammar Hideur, Alain Braud

Optics Letters

Effect of doping concentration on the performance of 2.8 µm Er:CaF_2 lasers

Venkatesan Jambunathan,[1] Simone Normani,[1] Pavel Loiko,[1] Karel Veselský,[1,2] Liza Basyrova,[1,3] Abdelmjid Benayad,[1] Patrice Camy,[1] Ammar Hideur,[4] and Alain Braud[1,*]

[1]Centre de Recherche sur les Ions, les Matériaux et la Photonique (CIMAP), UMR 6252 CEA-CNRS-ENSICAEN, Université de Caen Normandie, 6 Boulevard Maréchal Juin, 14050 Caen Cedex 4, France
[2]Faculty of Nuclear Sciences and Physical Engineering, Czech Technical University in Prague, Břehová 7, 115 19 Prague, Czech Republic
[3]FEMTO-ST Institute, Université de Franche-Comté, ENSMM, 26 rue de l'Epitaphe, 25000 Besançon, France
[4]CORIA UMR6614, CNRS-INSA-Université de Rouen, Normandie Université, Avenue de l'université, BP. 12, 76801 Saint Etienne du Rouvray, France
*alain.braud@ensicaen.fr

Received 14 January 2025; revised 23 February 2025; accepted 3 March 2025; posted 3 March 2025; published 13 March 2025

The effect of rare-earth doping on the spectroscopy and mid-infrared laser performance of Er^{3+}:CaF_2 crystals was investigated. An optimum doping level of 3–5 at.% was identified owing to ion clustering. Pumped by a high-brightness Yb-fiber laser at 976 nm, a continuous-wave 5 at.% Er^{3+}:CaF_2 laser generated 1.22 W at 2798 nm with a slope efficiency of 38.3% exceeding the Stokes limit, and the laser wavelength was continuously tunable across 2690–2830 nm (tuning range: 140 nm). The ratio of energy-transfer upconversion rates from $^4I_{11/2}$ and $^4I_{13/2}$ states was quantified relating to the energy recycling process.

https://doi.org/10.1364/OL.555586

In the past years, compact, efficient, and broadly tunable coherent light sources emitting around 3 µm garnered significant attention due to their vast application potential in medicine, molecular spectroscopy, and frequency downconversion toward mid-infrared, e.g., in transition-metal ion lasers [1] and supercontinuum sources [2]. Several rare-earth ions emit within this spectral range, comprising Er^{3+}, Ho^{3+}, and Dy^{3+} [3–6]. Among them, 3-µm lasers exploiting the $^4I_{11/2} \rightarrow {}^4I_{13/2}$ transition of erbium ions (Er^{3+}) benefit from efficient pumping at 0.98 µm directly to the upper laser level by commercial high-power InGaAs laser diodes or high-brightness Yb-fiber lasers [7,8]. The aforementioned Er^{3+} laser transition has a self-terminating nature, as the luminescence lifetime of the terminal laser manifold is usually longer than that of the upper laser level (with the latter being subject to a significant multiphonon non-radiative relaxation). Consequently, low-phonon laser gain media, such as fluoride crystals [9] and glasses (in the form of fibers [10]) are highly sought after. High-power 3-µm Er:ZBLAN fiber lasers exist, but the fluoride fiber technology remains challenging.

The true continuous-wave (CW) 3-µm operation of Er lasers is enabled by an energy-transfer upconversion (ETU) process, $^4I_{13/2} + {}^4I_{13/2} \rightarrow {}^4I_{9/2} + {}^4I_{15/2}$, recycling the energy of electronic excitation and mitigating the bottleneck effect [11]. In crystals with an isomorphic substitution of activator centers, such as cubic garnets [12,13], represented by Er:$Y_3Sc_2Ga_3O_{12}$ (shortly Er:YSGG), a commonly used material for 3-µm lasers, the ETU rate is boosted by increasing the doping level, typically to 30–40 at.% Er^{3+}. However, this is accompanied by a degradation of thermal properties of the gain material leading to severe thermal effects [14].

Another strategy for enhancing the energy-transfer processes among the activator ions relies on crystals with ion clustering. One remarkable example is the calcium fluoride (CaF_2) crystal. When the rare-earth doping level surpasses a certain limit, about 0.5 at.%, the majority of ions tend to reside in close proximity to one another, forming clusters of RE^{3+}–F_i^- pairs (with interstitial fluorine anions F_i^- serving for charge compensation) [15]. This leads to significant inhomogeneous spectral line broadening. In addition, it exhibits superior thermal properties and higher rare-earth ion solubility for CaF_2 over its glass counterparts (ZrF_4 and InF_3 based glasses). Yb^{3+}:CaF_2 has been recognized as an excellent material for femtosecond high-power/energy lasers at 1 µm [16]. Three-micrometer lasers based on Er^{3+}:CaF_2 have gained attention in the past, and recent works have shown power scaling capabilities [17–20]: remarkably, Zhu *et al.* reported on a diode-pumped 3 at.% Er^{3+}:CaF_2 laser delivering 14.5 W at 2796 nm with a slope efficiency of 24.9% [20].

In the present work, we aimed to assess the effect of the doping level varied over a broad range of 0.05–10 at.% on the spectroscopy and mid-infrared laser performance of Er^{3+}:CaF_2 crystals pumped by a high-brightness 976-nm Yb-fiber laser.

A series of Er^{3+}-doped CaF_2 single crystals was grown by the Bridgman–Stockbarger method using graphite crucibles (Ø8 mm, height: 40 mm). The starting reagents were CaF_2 (purity: 4N, *Sigma-Aldrich*) and ErF_3 obtained via fluorination of an Er_2O_3 powder (4N, *Alfa Aesar*). The doping level was 0.05 at.% to 10 at.% Er^{3+} (with respect to Ca^{2+}). To avoid

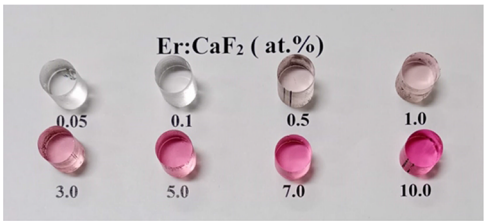

Fig. 1. Photograph of laser-grade polished Er:CaF_2 crystal samples with different doping levels (0.05–10 at.%).

any oxygen contamination of the crystals, the growth chamber was sealed to vacuum ($<10^{-5}$ mbar) and refilled with $Ar + CF_4$ gases. The crucible with the growth charge was first heated above (~30–50°C) the melting point (1418°C) for 3–4 h to homogenize the solution. Then, the temperature was reduced, and the growth was ensured by a vertical translation of the crucible in a temperature gradient of 30–40°C/cm. After completing the growth, the crystals were slowly cooled down to room temperature, during 48 h. No post-growth annealing was applied. Cylindrical crystals with a uniform cross section (Ø7 mm, length: 30–35 mm) were obtained. They exhibited gradually increasing coloration (from blank to deep pink) for higher Er^{3+} doping levels, Fig. 1. The crystals were transparent and of high optical quality.

Prior to laser experiments, we performed a spectroscopic study of Er^{3+}:CaF_2 crystals focusing on the effect of doping. Figure 2(a) displays the energy-level diagram of Er^{3+} showing the processes relevant for 2.8-μm lasers. The luminescence lifetimes τ_{lum} of the upper and lower laser manifolds were measured under resonant excitation ($^4I_{11/2}$: $\lambda_{exc} = 970$ nm, $\lambda_{lum} = 1020$ nm; $^4I_{13/2}$: $\lambda_{exc} = 1475$ nm, $\lambda_{lum} = 1580$ nm) (Fig. 2(b)). Finely powdered samples were used to avoid radiation trapping. The concentration dependences are complex due to a combination of i) redistribution of Er^{3+} ions over different sites (ion clustering) and ii) concentration quenching. For the $^4I_{11/2}$ level, τ_{lum} is relatively long owing to the low-phonon energy of the host matrix and varies in the range of 8.64–3.41 ms for the range of doping levels of 0.05–10 at.%. Such long lifetimes would favor the low-threshold laser operation. The lifetime ratio, $\tau_{lum}(^4I_{11/2})/\tau_{lum}(^4I_{13/2})$, was further calculated, reaching almost 2 for 5 at.% Er^{3+} doping. This case represents the most favorable scenario for avoiding the bottleneck effect for laser operation.

The evolution of Er^{3+} absorption at 0.98 μm (the $^4I_{15/2} \rightarrow {}^4I_{11/2}$ pump transition), as well as its mid-infrared luminescence at 2.8 μm (the $^4I_{11/2} \rightarrow {}^4I_{13/2}$ laser transition), was then studied (Figs. 2(c) and 2(d)). For low doping of ≤0.1 at.%, the spectra are dominated by Er^{3+} ions residing in isolated sites (tetragonal, C_4 v; trigonal, C_3 v; and cubic, O_h), and for higher doping levels, the spectra inhomogeneously broaden due to ion clustering. One can see the formation of more complex clusters as the spectra continue to evolve until Er^{3+} content up to 3 at.%. For higher Er^{3+} doping, the absorption cross section, σ_{abs}, is 0.21×10^{-20} cm^2 at 981.3 nm, and the absorption bandwidth (full width at half maximum, FWHM) reaches 21 nm (see Fig. 2(c)). In the spectral range where a laser operation is expected, the stimulated-emission cross section, σ_{SE}, is calculated to be 0.36×10^{-20} cm^2 around 2800 nm, and the emission bandwidth is 122 nm. Based on the performed spectroscopic study, we conclude that 3–5 at.% Er^{3+}-doped CaF_2 crystals appear most promising for low-threshold broadly tunable (and potentially mode-locked) lasers as they combine an attractive

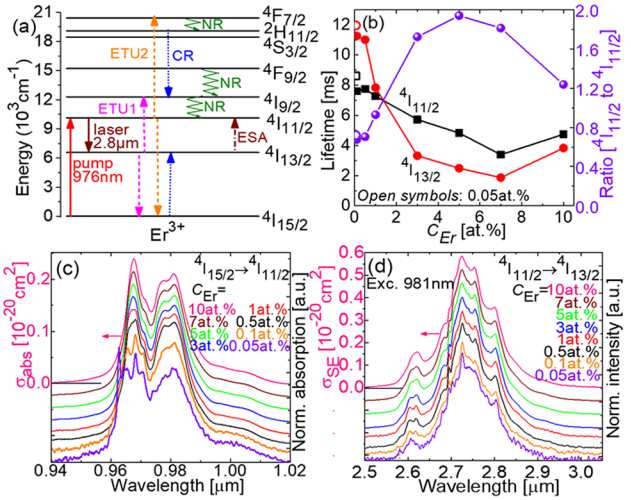

Fig. 2. Concentration-dependent spectroscopic study of Er^{3+} ions in CaF_2 crystals: (a) partial Er^{3+} energy-level scheme, ETU, energy-transfer upconversion; CR, cross-relaxation; ESA, excited-state absorption; NR, non-radiative decay; (b) luminescence lifetimes of the $^4I_{11/2}$ and $^4I_{13/2}$ levels; (c) evolution of absorption spectra at 0.98 μm, the $^4I_{15/2} \rightarrow {}^4I_{11/2}$ transition; (d) evolution of emission spectra at 2.8 μm, the $^4I_{11/2} \rightarrow {}^4I_{13/2}$ transition. In (c) and (d), the absorption, σ_{abs}, and stimulated-emission, σ_{SE}, cross sections are given for 10 at.% Er^{3+} doping.

ratio of the upper-to-lower laser level lifetimes with broad and smooth mid-infrared emission profiles.

The layout of the laser setup is depicted in Fig. 3(a). Cylindric laser elements were cut from the central parts of Er^{3+}:CaF_2 crystal boules having a diameter of 7 mm and a thickness of 6–7 mm. They were polished to laser-grade quality with a parallelism better than 15′ and left uncoated. A total of seven samples with the doping level C_{Er} ranging from 0.1 to 10 at.% Er were tested. The samples were mounted in a passively cooled Cu holder using a thermal conductive silver paint for better heat removal. The nearly hemispherical linear laser cavity consisted of a plane dichroic pump mirror (PM) coated for high transmission (HT) at 0.98 μm and high reflection (HR) at 2.6–3.0 μm and a set of concave output couplers (OC) having a radius of curvature of −100 mm and a transmission at the laser wavelength T_{OC} in the range of 0.33–4.0%. The crystal was placed near the PM leaving a small air gap of less than 1 mm. The total cavity length was 99 mm. The pump source was a commercial Yb-fiber laser (*Azurlight Systems*, ALS-IR-122) with an in-built collimator that was protected from back-reflected pump by an optical isolator. The maximum incident pump power was about 6 W at 975.8 nm (linewidth: 0.3 nm) with a nearly diffraction-limited beam quality (measured $M^2 = 1.02$). The pump source addressed the $^4I_{15/2} \rightarrow {}^4I_{11/2}$ Er^{3+} transition. The pump radiation was focused into the crystal through the dichroic mirror using an antireflection (AR) coated achromatic lens (focal length: $f = 75$ mm). The pumping was in single pass. The measured pump absorption (cf. Figure 3(b)) gradually increased with the Er doping level, from 5% for 0.1 at.% Er to 90% for 10 at.% Er. The residual pump after the OC was filtered using a long-pass filter (LP2400, *Spectrogon*). The laser emission spectra were measured by an optical spectrum analyzer (*Yokogawa* AQ6376) and a ZrF_4 fiber (*Thorlabs*). The far-field beam profile was captured using a pyroelectric camera (PY-III-HR-C-A, *Ophir-Spiricon*).

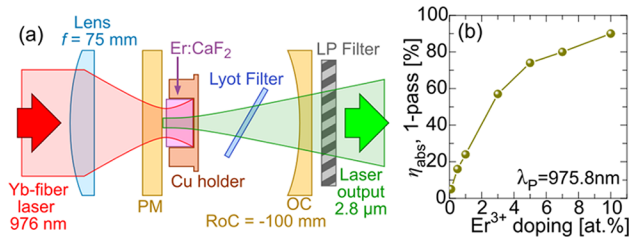

Fig. 3. (a) Laser setup: PM, pump mirror, OC, output coupler; (b) single-pass pump absorption in Er^{3+}:CaF_2 crystals with different doping levels.

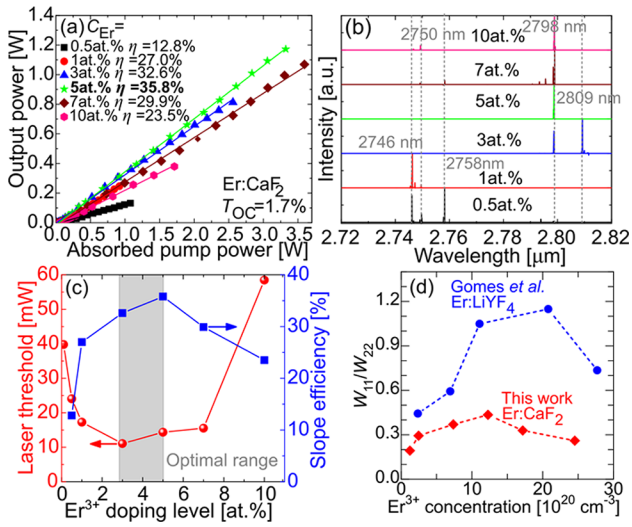

Fig. 4. Effect of the doping level on the 2.8-μm performance of Er^{3+}:CaF_2 lasers pumped by an 976-nm Yb-fiber laser: (a) power transfer curves, η—slope efficiency; (b) typical laser emission spectra measured well above the laser threshold; (c) evolution of the laser threshold and slope efficiency versus the Er^{3+} doping level, $T_{OC} = 1.7\%$; (d) the ratio of ETU rates from the two laser manifolds, W_{11}/W_{22}, as a function of the doping level calculated using Eq. (1), in comparison with Er:$LiYF_4$ [23].

A continuous-wave laser operation at 2.8 μm was achieved for the entire range of the studied Er^{3+} doping levels except for very low-doped samples ($C_{Er} \le 0.1$ at.%). In the first set of experiments, the output coupling was fixed at 1.7%, and the power transfer curves were measured for various crystals (see Fig. 4(a)). On increasing the doping level, an increased pump absorption first allowed for better power scaling. However, for $C_{Er} > 5$ at.%, the thermal effects in the laser crystal limited the available pump power as a thermal roll-over was observed, e.g., above an absorbed pump power of 3.5 W for $C_{Er} = 7$ at.%. Moreover, for $C_{Er} = 10$ at.%, the laser crystal suffered a thermal fracture at an absorbed pump power of ~2 W. The best output performance was obtained for the 5 at.% Er^{3+}-doped crystal. The laser generated a maximum output power of 1.17 W at 2798 nm with a slope efficiency η of 35.8% (versus the absorbed pump power, P_{abs}) and a laser threshold of only 14 mW. This corresponded to an incident pump power of 4.49 W and an overall optical efficiency of 26.0%. The input–output dependence was linear up to at least P_{abs} of 3.3 W, and no detrimental thermal effects were observed in this range of pump powers.

The typical spectra of laser emission are shown in Fig. 4(b). For C_{Er} above 1 at.%, the laser operated at longer wavelengths, notably 2798 and 2809 nm (due to the stronger reabsorption from the long-living terminal laser level, $^4I_{13/2} \rightarrow {}^4I_{11/2}$), while for low Er^{3+} doping, three laser lines appeared at 2746, 2750, and 2758 nm. The laser emission was unpolarized.

Figure 4(c) shows the evolution of laser slope efficiency and laser threshold with the Er^{3+} doping level. Both parameters were optimized in the range of Er^{3+} concentrations of 3–5 at.%. Pollnau *et al.* proposed an expression for the slope efficiency of 3-μm Er lasers accounting for the energy recycling due to the ETU processes [21]:

$$\eta = \eta_{St,L} \frac{\ln(1 - T_{OC})}{\ln[(1 - T_{OC})(1 - L)]} \left(2 - \frac{b_1^2}{b_2^2} \frac{W_{22}}{W_{11}}\right), \quad (1)$$

where $\eta_{St,L} = \lambda_P/\lambda_L$ is the Stokes efficiency under lasing conditions; λ_P (λ_L) are the pump (laser) wavelengths; L is the round trip passive loss; W_{11} and W_{22} are the ETU rates from the $^4I_{13/2}$ and $^4I_{11/2}$ Er^{3+} laser manifolds, respectively; and b_1 and b_2 are the Boltzmann factors of the Stark sublevels of the $^4I_{13/2}$ and $^4I_{11/2}$ multiplets responsible for the laser transition. This formula assumes a mode-matching efficiency close to unity. If $W_{22} = 0$, the formula indicates an upper limit for the laser slope efficiency of $2\eta_{St,L}$ (a two-for-one pump process). Using this equation, we computed the ratio of the ETU rates W_{11}/W_{22}, as shown in Fig. 4(d). The Stark splitting for Er^{3+} ions in clusters in CaF_2 was reported by Normani *et al.* [22] yielding $b_1 = 0.138$ and $b_2 = 0.254$, and the L value of 0.5% was estimated using the Caird analysis. The maximum W_{11}/W_{22} ratio of 0.43, corresponding to the highest slope efficiency, is found for the 5 at.% Er^{3+}-doped CaF_2 crystal (the corresponding ion density N_{Er} is 12.3×10^{20} cm^{-3}). For comparison, we also show the W_{11}/W_{22} ratios for an ordered Er:$LiYF_4$ crystal, which is also commonly used in 2.8-μm Er lasers (the values are derived from the spectroscopic measurements performed by Gomes *et al.* [23]). Here, the optimal value of the Er^{3+} doping level is around 15 at.% ($N_{Er} = 20.8 \times 10^{20}$ cm^{-3}), where the W_{11}/W_{22} ratio reaches 1.15. This analysis allows us to draw two conclusions: i) the ion clustering in Er^{3+}:CaF_2 crystals accelerates the energy-transfer processes shifting the optimum concentration to lower doping levels (as compared to Er^{3+}:$LiYF_4$ crystals with isomorphic distribution of activator impurity centers); and ii) the relatively strong ETU from the $^4I_{11/2}$ manifold in Er^{3+}:CaF_2 is the main limiting factor for boosting the laser slope efficiency far beyond the Stokes limit.

We further studied the best-performing 5 at.% Er^{3+}:CaF_2 crystal with different output coupler transmissions (Fig. 5(a)). A maximum output power of 1.22 W at 2798 nm was achieved with $\eta = 38.3\%$ (for 4% OC). The laser threshold gradually decreased from 64 to less than 10 mW on decreasing T_{OC} from 4.0 to 0.33%. The laser operated at 2798 nm (except for the very low 0.33% OC for which the emission occurred at a slightly longer wavelength of 2811 nm). The Er laser operated at the fundamental transverse mode with a measured beam quality factor M^2 of ~1.2. Figure 5(c) depicts the measured far-field beam profile at the maximum output power. The high laser slope efficiencies achieved in this work are assigned to i) an optimized Er^{3+} doping (the W_{11}/W_{22} ratio), ii) high-brightness pumping by an Yb-fiber laser and, therefore, good mode matching, and iii) high optical quality of the grown crystals.

To explore the wavelength tuning potential of the Er^{3+}:CaF_2 crystal, a birefringent filter (BRF) was inserted in the laser cavity

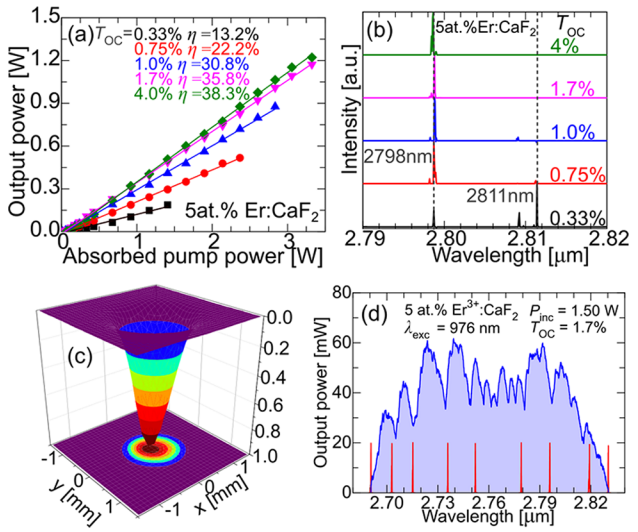

Fig. 5. 2.8-µm 5 at.% Er^{3+}:CaF_2 laser: (a) input–output dependences for different output coupling, η—slope efficiency; (b) typical laser emission spectra measured well above the laser threshold; (c) a typical far-field beam profile measured at the maximum output power; (d) wavelength tuning curve, *red curves*—example laser spectra, T_{OC} = 1.7%.

close to the crystal at Brewster's angle. It comprised a 0.8-mm-thick uncoated MgF_2 plate with the optical axis lying in the plane of the filter. The free spectral range of the filter was 290 nm. The BRF was mounted in a computer controlled rotatory stage (*SmarAct*) with an angular step of 50 µdeg. The output power and the laser wavelength were simultaneously measured for each BRF position. The Er^{3+}:CaF_2 laser was continuously tunable from 2690 to 2830 nm (tuning range of 140 nm at a zero power level) (Fig. 5(d)). The dips in the tuning curve are due to the structured absorption of water vapors in the air.

The maximum solubility of ErF_3 in CaF_2 retaining the cubic phase is relatively high, about 40 mol% [24]. In practice, doping levels above 10 at.% Er^{3+} would cause a significant drop in the thermal conductivity of such solid-solution compounds [25] and further shortening of the luminescence lifetimes due to energy migration.

To conclude, rare-earth ion clustering in Er^{3+}-doped low-phonon energy CaF_2 crystals makes them exceptionally suitable for 2.8-µm mid-infrared lasers based on energy recycling. The clustering effect leads to inhomogeneously broadened spectral gain profiles supporting continuous wavelength tuning over 140 nm (2690–2830 nm) and, potentially, femtosecond pulse generation from mode-locked lasers operating under anhydrous atmosphere. It shifts the optimum Er^{3+} doping level down to 3–5 at.% with respect to crystals with an isomorphic distribution of activator ions such as $LiYF_4$ or YSGG requiring doping levels of tens of at.%, which is essential for maintaining the good thermal properties of laser crystals. We identify the strong ETU from the upper laser level ($^4I_{11/2}$) as a main limiting factor for energy recycling in Er^{3+}:CaF_2, but we still demonstrate laser slope efficiencies above the Stokes limit. Remarkably, we have demonstrated a CW laser operation with low-doped crystals (≤0.5 at.% Er^{3+}), which opens what we believe to be a novel paradigm for low-doped crystal-rod fiber lasers.

Funding. Agence Nationale de la Recherche (ANR-22-CE08-0031, FLAMIR).

Disclosures. The authors declare no conflicts of interest.

Data availability. Data underlying the results presented in this paper are not publicly available at this time but may be obtained from the authors upon reasonable request.

Supplemental document. See Supplement 1 for supporting content.

REFERENCES

1. S. Mirov, V. Fedorov, I. Moskalev, *et al.*, Laser Photonics Rev. **4**, 21 (2010).
2. T. S. Saini, N. P. Trung Hoa, K. Nagasaka, *et al.*, Appl. Opt. **57**, 1689 (2018).
3. R. I. Woodward, M. R. Majewski, G. Bharathan, *et al.*, Opt. Lett. **43**, 1471 (2018).
4. R. Švejkar, J. Šulc, and H. Jelínková, Progr. Quantum Electron. **74**, 100276 (2020).
5. J. Li, D. D. Hudson, and S. D. Jackson, Opt. Lett. **36**, 3642 (2011).
6. J. Wang, X. Zhu, R. A. Norwood, *et al.*, Opt. Express **29**, 38646 (2021).
7. S. D. Jackson, T. A. King, and M. Pollnau, Opt. Lett. **24**, 1133 (1999).
8. F. Cassouret, A. Nady, P. Loiko, *et al.*, Opt. Lett. **49**, 2970 (2024).
9. C. Labbé, J. L. Doualan, P. Camy, *et al.*, Opt. Commun. **209**, 193 (2002).
10. S. Tokita, M. Murakami, S. Shimizu, *et al.*, Opt. Lett. **34**, 3062 (2009).
11. M. Pollnau, T. Graf, J. E. Balmer, *et al.*, Phys. Rev. A **49**, 3990 (1994).
12. B. J. Dinerman and P. F. Moulton, Opt. Lett. **19**, 1143 (1994).
13. S. Normani, P. Loiko, Z. Pan, *et al.*, Opt. Lett. **48**, 2567 (2023).
14. J. Wang, T. Cheng, L. Wang, *et al.*, Laser Phys. Lett. **12**, 105004 (2015).
15. V. Petit, P. Camy, J.-L. Doualan, *et al.*, Phys. Rev. B **78**, 085131 (2008).
16. F. Druon, S. Ricaud, D. N. Papadopoulos, *et al.*, Opt. Mater. Express **1**, 489 (2011).
17. J. Šulc, M. Němec, R. Švejkar, *et al.*, Opt. Lett. **38**, 3406 (2013).
18. L. Basyrova, P. Loiko, J. L. Doualan, *et al.*, Opt. Express **30**, 8092 (2022).
19. M. Zong, Y. Wang, Z. Zhang, *et al.*, J. Lumin. **250**, 119089 (2022).
20. L. Zhu, Z. Zhang, Y. Wang, *et al.*, Opt. Lett. **49**, 4286 (2024).
21. M. Pollnau, R. Spring, C. Ghisler, *et al.*, IEEE J. Quantum Electron. **32**, 657 (1996).
22. S. Normani, P. Loiko, L. Basyrova, *et al.*, Opt. Mater. Express **13**, 1836 (2023).
23. L. Gomes, A. F. H. Librantz, F. H. Jagosich, *et al.*, J. Appl. Phys. **106**, 103508 (2009).
24. B. P. Sobolev and P. P. Fedorov, J. Less Common Met. **60**, 33 (1978).
25. P. A. Popov, P. P. Fedorov, S. V. Kuznetsov, *et al.*, Dokl. Phys. **53**, 198 (2008).